Nonoxidative Conversion of Methane in a Dielectric Barrier Discharge Reactor: Prediction of Reaction Performance Based on Neural Network Model

ARTICLE *in* THE JOURNAL OF PHYSICAL CHEMISTRY C · MAY 2014

Impact Factor: 4.77 · DOI: 10.1021/jp502557s

4 AUTHORS, INCLUDING:

Shiyun Liu
University of Liverpool
3 PUBLICATIONS **6** CITATIONS
SEE PROFILE

Danhua Mei
University of Liverpool
11 PUBLICATIONS **77** CITATIONS
SEE PROFILE

Xin Tu
University of Liverpool
58 PUBLICATIONS **751** CITATIONS
SEE PROFILE

THE JOURNAL OF PHYSICAL CHEMISTRY C

Article

pubs.acs.org/JPCC

Nonoxidative Conversion of Methane in a Dielectric Barrier Discharge Reactor: Prediction of Reaction Performance Based on Neural Network Model

S. Y. Liu, D. H. Mei, Z. Shen, and X. Tu*

Department of Electrical Engineering and Electronics, University of Liverpool, Brownlow Hill, Liverpool, L69 3GJ, U.K.

ABSTRACT: The nonoxidative conversion of CH_4 into H_2 and higher hydrocarbons has been performed in a coaxial dielectric barrier discharge reactor at atmospheric pressure and low temperatures. The effect of discharge power, gas flow rate, and excitation frequency on the reaction performance of the plasma methane conversion is investigated. A three-layer back-propagation artificial neural network (ANN) model has been developed and trained to simulate and predict the complex plasma chemical reaction in terms of the conversion of CH_4, the selectivity and yield of gas products, and the energy efficiency of the plasma process. A good agreement between the experimental and simulated results is achieved. The ANN model shows that the maximum CH_4 conversion of 36% can be obtained at a discharge power of 75 W with a high selectivity of C_2H_6 (42.4%). In this study, the discharge power is found to be the most influential parameter with a relative weight of 45−52% for the plasma nonoxidative coupling of methane, while the excitation frequency of the plasma system is the least important parameter affecting the plasma process. The results successfully demonstrate that the well-trained ANN model can accurately simulate and predict a complex plasma chemical reaction.

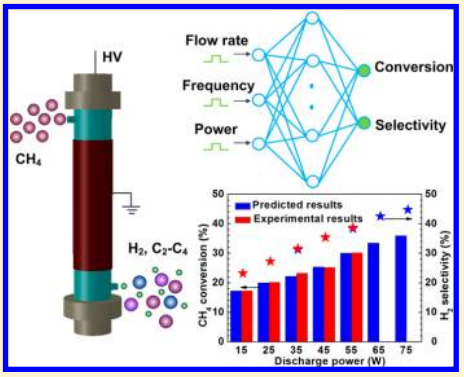

1. INTRODUCTION

The growing energy demand in modern society together with decreasing reserves of fossil fuel have accentuated the urgent need to develop alternative and renewable energy sources. Moreover, there has been a growing concern worldwide about climate change and global warming caused by the consumption of fossil fuel and greenhouse gas emissions. Hydrogen is considered to be an attractive, clean, and key energy carrier which can support sustainable economic growth. It can be used to generate electricity by combustion in an internal combustion engine (ICE) or by the use of fuel cells, where chemical energy is converted into electricity in an electrochemical cell. The latter is favorable, particularly for automotive applications, given that the transfer of chemical energy associated with fuel cells is more efficient and clean than methods of combustion where loss of energy as heat is inevitable.[1] Hydrogen can be produced from a variety of resources (water, fossil fuel and biomass) with different technologies.

Methane is a major component of natural gas and biogas. The Intergovernmental Panel on Climate Change (IPCC) reports that, over a 20-year time frame, methane has a global warming potential of 86 compared to that of CO_2.[2] The conversion of abundant methane with and without using oxidants into hydrogen and value-added chemicals such as higher hydrocarbons and methanol has exhibited promising potential and attracted great interest.[3−5] Although direct activation of methane with the aid of oxidants is thermodynamically more favorable than nonoxidative conversion of methane, a particular advantage for the later route is the production of CO_x free, hydrogen-rich gases, which is of great interest to the development of highly efficient and cost-effective fuel cells.

However, methane is the most stable and symmetric organic molecule, consisting of four C−H bonds with bond energy of 435 kJ/mol, which presents a challenge for conversion by a conventional thermal catalytic process.[5] Thermodynamic equilibrium calculations showed that nonoxidative coupling of methane almost cannot occur at room temperature.[5] High energy input is required to activate chemical bonds of CH_4 molecule at high reaction temperatures (>700 °C). The formation of carbon deposition on the surface of catalysts leads to the fast deactivation of catalysts, especially for supported non-noble metal catalysts.

Nonthermal plasma technology offers an attractive and promising alternative to the conventional catalytic route for the conversion of methane into higher-value fuels and chemicals at atmospheric pressure and low temperatures.[6−16] In nonthermal plasmas, the overall gas kinetic temperature can be as low as room temperature, while the electrons are highly energetic with a typical electron temperature of 1−10 eV, which can easily break down inert molecules and produce a variety of species: free radicals, excited atoms, ions, and molecules for subsequent physical and chemical reactions.[17−19] Nonthermal plasmas could break thermodynamic barrier in high-temperature chemical reactions and enable thermodynamically unfavorable

Received: March 13, 2014
Revised: April 18, 2014
Published: May 7, 2014

dx.doi.org/10.1021/jp502557s | J. Phys. Chem. C 2014, 118, 10686−10693

reactions to occur under ambient conditions.[20] Considerable efforts have been dedicated to investigating the effectiveness of methane conversion by using a variety of plasma sources such as dielectric barrier discharge (DBD), corona discharge, glow discharge, gliding arc, and spark discharge.[21−34] However, nonoxidative conversion of CH_4 into hydrogen and higher hydrocarbons without using dilution gas has received little attention in previous literature. Plasma processing of methane is very complicated and a fundamental understanding of the underlying physical and chemical reactions is very limited, making it difficult to optimize processing parameters and predict the selectivity and yield of end products theoretically. Developing a comprehensive plasma physical and chemical kinetic model offers an attractive route for solving this problem.[35−38] De Bie et al. developed a 1D fluid model to elucidate the plasma chemistry in the nonoxidative conversion of CH_4 using a dielectric barrier discharge.[36,37] The model consists of 36 species (electrons, atoms, ions, molecules) and 367 gas-phase reactions. In our recent work, a zero-dimensional chemical kinetic model involving 498 reactions and 62 species has been developed to understand the chemical mechanisms and reaction pathways of the plasma-based dry reforming of methane.[38] However, comprehensive modeling of plasma chemical reactions needs an efficient and robust numerical solver and is a time-consuming process, which is not desirable for the fast and reliable prediction and optimization of highly complex plasma processes.

Artificial neural networks (ANNs) have been considered as a promising and powerful tool for simulation, prediction, and optimization of complex and nonlinear process systems. ANNs offer a number of advantages, including requiring less formal statistical training, the ability to implicitly detect complex and nonlinear relationships between dependent and independent variables, the ability to detect all possible interactions between predictor variables, and the availability of multiple training algorithms.[39] However, there are very few studies on the application of ANNs to simulate plasma chemical reactions.

In this study, the plasma nonoxidative conversion of CH_4 into hydrogen and higher hydrocarbons has been investigated in a dielectric barrier discharge reactor under ambient conditions. An ANN model has been developed to get new insights into the effect and relative importance of different processing parameters on the reaction performance of the plasma methane conversion and to predict the complex plasma chemical reaction in terms of the conversion of CH_4, the selectivity and yield of gas products, and the energy efficiency of the plasma process. The possible reaction mechanisms leading to the formation of major gas products are discussed.

2. EXPERIMENT AND NEURAL NETWORK MODEL

2.1. Experimental Setup. The experiment is carried out in a coaxial DBD reactor, as shown in Figure 1. The outer electrode of the reactor is connected to a high-voltage output, and the inner electrode is grounded via an external capacitor. The length of the plasma area is 90 mm with a discharge gap of 2 mm. Pure CH_4 is used as the feed gas with a gas flow rate of 50−300 mL min^{-1}. The DBD reactor is water-cooled to control the gas temperature (<80 °C) of the methane discharge. The plasma reactor is supplied by an AC high-voltage power supply with a variable frequency of 20−50 kHz. The applied voltage is measured by a high-voltage probe (Tektronics P6015A), while the current is sampled by a current monitor (Pearson 4100). All the electrical signals are recorded by a 500 MHz digital oscilloscope (Tektronics TDS3052). The gas products of the plasma reaction are analyzed by a gas chromatography (GC, Interscience) instrument equipped with a flame ionization detector (FID) and two thermal conductivity detectors (TCDs).

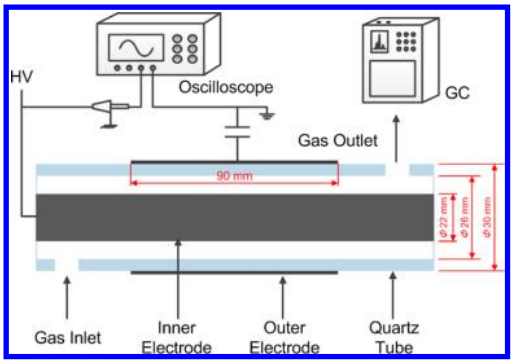

Figure 1. Schematic diagram of the experimental system.

For the nonoxidative conversion of methane, the conversion of CH_4 is defined as

$$C_{CH_4}(\%) = \frac{\text{moles of } CH_4 \text{ converted}}{\text{moles of } CH_4 \text{ input}} \times 100 \quad (1)$$

The selectivities S and yields Y of the gas products can be calculated as follows:

$$S_{H_2}(\%) = \frac{\text{moles of } H_2 \text{ produced}}{2 \times \text{moles of } CH_4 \text{ converted}} \times 100 \quad (2)$$

$$S_{C_xH_y}(\%) = \frac{x(\text{moles of } C_xH_y \text{ produced})}{\text{moles of } CH_4 \text{ converted}} \times 100 \quad (3)$$

$$Y_{H_2}(\%) = \frac{\text{moles of } H_2 \text{ produced}}{2(\text{moles of } CH_4 \text{ input})} \times 100 \quad (4)$$

$$Y_{C_xH_y}(\%) = \frac{x(\text{moles of } C_xH_y\text{produced})}{\text{moles of } CH_4\text{input}} \times 100 \quad (5)$$

The energy efficiency of a plasma reactor for the conversion of CH_4 is defined as the number of moles of methane converted per unit of discharge power:

$$\text{energy efficiency (mol/J)} = \frac{\text{moles of } CH_4 \text{ converted}}{\text{power}} \quad (6)$$

2.2. Artificial Neural Network. An artificial neural network is a computing system composed of a number of highly interconnected neurons or processing elements, which process information by their dynamic state response to external inputs.[40] The neural network maps a set of input patterns onto a corresponding set of output patterns. A typical ANN consists of multiple layers including an input layer, one or more hidden layers, and an output layer. Each layer is composed of one or more neurons and communication paths between them. The function of the input layer is to receive information from an external source and pass this information to the network for processing, while the role of the output layer is to receive processed information from the network and send the results out to an external receptor. Between the input and output layers are one or more hidden layers, each consisting of a number of neurons which process all of the information from the input layer. ANN works very well for the analysis of

dx.doi.org/10.1021/jp502557s | J. Phys. Chem. C 2014, 118, 10686−10693

classification problems in the engineering field because of its excellent ability to self-learn, self-organize, and self-adapt.

In this work, the MATLAB neural network toolbox is used to design and train a neural network for modeling the plasma methane reaction. The experimental data are split into two groups: an input set X and a target output set T. Three different processing parameters—discharge power, excitation frequency, and gas flow rate—are identified as input variables in the ANN model, while the output variables include the conversion of CH_4 and selectivity of H_2, C_2H_2/C_2H_4, C_2H_6, C_3H_8, and C_4H_{10}. The yield of gas products and energy efficiency of the plasma process can be calculated from the calculated output variables. In addition, the experimental data are randomly divided into training and test sets. The training set is used to determine and adjust the connection weights between different layers, while the test set is used to evaluate the accuracy and performance of the ANN model. An optimal and well-trained ANN model can be obtained when an error function between the actual outputs of the network and the target outputs reaches a minimum level.

3. RESULTS AND DISCUSSION

3.1. Neural Network Modeling. *3.1.1. Selection of Back-Propagation Training Algorithm.* Back-propagation (BP) is one of the most widely used supervised learning algorithms for the training of feed-forward multilayer neural networks. One of the advantages of this algorithm is that BP neural network has the ability to learn the desired relationship between input and output data through a training process, which is usually formulated as the minimization of an error such as the mean square error (MSE) between target outputs (experimental data) and actual outputs (simulated data) by iteratively adjusting connection weights between layers. The performance of the training process is accessed by an independent test data set.

In our previous work, we designed a three-layer feed-forward neural network and examined the model performance by using different BP algorithms.[41] The Levenberg–Marquardt (LM) training algorithm showed the best predictive performance of the neural network compared to that of other BP algorithms, which is consistent with other studies.[42,43] In this study, the LM algorithm with different combinations of transfer functions is used for the training of the neural network to get the optimal configuration of the neural network, which could provide a reliable and accurate prediction for the plasma conversion of CH_4 (Table 1). The performance of the neural network is evaluated in terms of the MSE and standard deviation error (SDE) between the actual outputs Y (simulated data) and target outputs T (experimental data),

$$\mathrm{MSE} = \frac{1}{N}\sum_{i=1}^{N}(T_i - Y_i)^2 \tag{7}$$

$$\mathrm{SDE} = \sqrt{\frac{1}{N}\sum_{i=1}^{N}(E_i - \bar{E})^2} \tag{8}$$

where N is the total number of the experimental samples used in the ANN. E_i is the absolute output error between the actual output and target output for the ith sample, and $\bar{E}$ refers to the mean value of the total output errors. Table 2 shows the MSE and SDE of the LM training algorithm combined with different transfer functions at the hidden and output layers. It is clear that the LM-TP configuration offers the best performance of the network with the least MSE and SDE.

Table 1. Tested Different Configurations of BP Neural Network

configuration	hidden layer function	output layer function	neuron number
LM-PT	linear	tangent sigmoid	3–10
LM-PP	linear	linear	3–10
LM-PL	linear	logarithm	3–12
LM-LT	logarithm	tangent sigmoid	3–12
LM-TT	tangent sigmoid	tangent sigmoid	3–12
LM-TP	tangent sigmoid	linear	3–12
LM-TL	tangent sigmoid	logarithm	3–12
LM-LL	logarithm	logarithm	3–10
LM-LP	logarithm	linear	3–10

Table 2. Best Performance for Each LM Configuration

configuration	MSE	correlation coefficient	SDE	best linear equation[a]
LM-PT	0.049 65	0.9998	0.1930	$Y = T + 0.11$
LM-PL	13.9554	0.9109	2.6977	$Y = 0.92T + 4.6$
LM-TP	0.047 95	0.999 82	0.1655	$Y = T + 0.035$
LM-LP	0.535 98	0.9998	0.2613	$Y = T + 0.0084$
LM-TL	2.0249	0.9748	1.9604	$Y = 0.95T + 2.1$
LM-LT	0.253 76	0.9988	0.4721	$Y = 0.95T + 2.1$
LM-TT	0.075 11	0.999 98	0.6430	$Y = T - 0.1$
LM-PP	0.553 49	0.9986	0.7149	$Y = T + 0.11$
LM-LL	8.8956	0.9488	2.7743	$Y = 0.94T + 3$

[a] Y is the predicted output set (simulated data); T is the target output set (experimental data).

3.1.2. Optimization of the Neuron Number. In this work, the LM training algorithm with a tangent sigmoid transfer function (TANSIG) at the hidden layer and a linear transfer function (PURELIN) at the output layer is used for training the BP neural network, as shown in Figure 2. The optimal neuron number at the hidden layer is determined based on the minimum MSE and SDE of the training set. We find the MSE and SDE values are 0.704 and 0.421, respectively, when 3

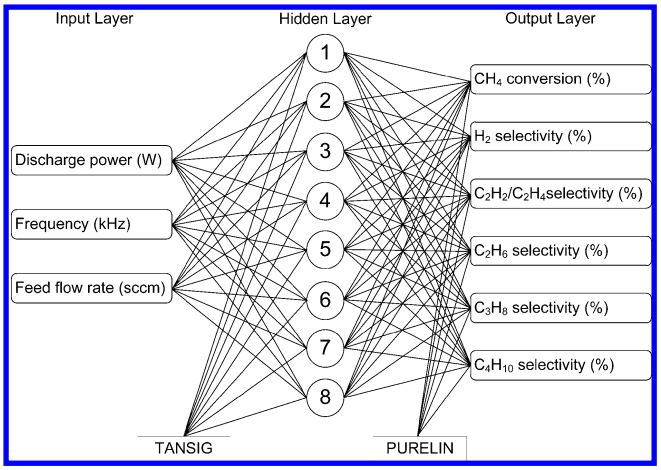

Figure 2. Optimized three-layer ANN model with a tangent sigmoid transfer function (TANSIG) at the hidden layer and a linear transfer function (PURELIN) at the output layer.

dx.doi.org/10.1021/jp502557s | J. Phys. Chem. C 2014, 118, 10686–10693

neurons are used at the hidden layer. Both values significantly decrease to 0.048 and 0.166, respectively, when 8 neurons are used. However, further increasing the neural number up to 12 does not reduce the MSE and SDE. Therefore, the optimal neuron number at the hidden layer for the LM-TP structure is determined to be 8.

3.1.3. Test and Validation of the Model. In this work, a three-layer BP neural network with a linear function at the hidden layer and a tangent sigmoid function at the output layer is used for the training of the neural network. A test data set that includes about 15% of the experimental data is used to feed the optimized ANN to evaluate the accuracy of the model. Figure 3 plots a comparison between the experimental data and

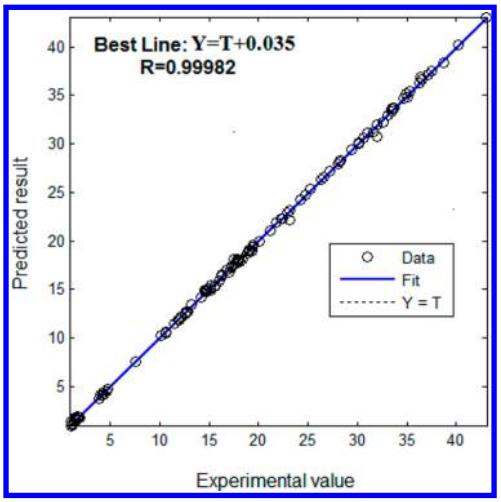

Figure 3. Comparison between the experimental data (target output set T) and predicted data (actual output set Y) for the optimzied ANN model.

predicted data from the LM-TP neural network model. The equation $Y = T$ represents the perfect fit line (dotted line), which means the simulated results are the same as the experimental data. The solid line shows the best-fit of the experimental data with the best linear equation $Y = T + 0.035$ with a correlation coefficient R^2 of 0.99982 and a MSE of 0.048. It is clear that there is a good agreement between the experimental results (target outputs) and predicted results (actual outputs).

3.1.4. Sensitivity Analysis. In this study, the neural net weight matrix and Garson equation are used to determine the relative importance of the plasma processing parameters.[42,43] This equation is based on the partitioning of connection weights of the optimal ANN model:

$$I_j = \frac{\sum_{m=1}^{m=N_h} ((|W_{jm}^{ih}|/\sum_{k=1}^{N_i}|W_{km}^{ih}|) \times |W_{mn}^{ho}|)}{\sum_{k=1}^{k=N_i}\{\sum_{m=1}^{m=N_h}(|W_{km}^{ih}|/\sum_{k=1}^{N_i}|W_{km}^{ih}|) \times |W_{mn}^{ho}|\}} \quad (9)$$

where I_j is the relative importance of the jth input variable for the whole process; N_i and N_h are the number of input and hidden neurons, respectively. W represents the connection weight. In addition, the superscripts i, h, and o refer to the input, hidden, and output layers, respectively, while the subscripts k, m, and n refer to the input, hidden, and output neurons.[42,43]

Table 3 presents the weights produced by the optimized ANN that are used in this work. The relative importance of the input parameters is determined by eq 9, as shown in Table 4. In this study, the discharge power has a significant impact on the reaction performance of the plasma process in terms of the conversion of CH_4 and the selectivity of gas products (H_2 and C_2-C_4). The gas flow rate is identified as the second important parameter for the plasma processing of methane, and the relative importance of this parameter (45%) on the methane conversion is comparable to that of the discharge power. In contrast, the excitation frequency contributes the least to the plasma process because of its lowest importance for all outputs.

Table 4. Relative Importance of Processing Parameters for the Optimized ANN Model

	relative importance (%)					
	conversion	selectivity				
input variable	CH_4	H_2	C_2H_2/C_2H_4	C_2H_6	C_3H_8	C_4H_{10}
frequency	9.7	10.8	17.5	12.9	14.1	13.0
flow rate	45.1	37.0	30.2	39.6	41.3	39.6
power	45.2	52.2	52.3	47.5	44.6	47.4
total	100	100	100	100	100	100

3.2. Plasma-Assisted Methane Conversion. *3.2.1. Effect of Gas Flow Rate.* Figure 4 shows a comparison between the predicted and experimental results for the plasma conversion of CH_4 at different gas flow rates. The simulated data obtained from the well-trained neural network model are in fairly good agreement with the experimental data. The gas flow rate shows a considerable impact on the plasma reaction performance,

Table 3. Weight Matrices W1 (Weights between Input and Hidden Layers) and W2 (Weights between Hidden and Output Layers)

	W1			W2					
	input variables			outputs (%)					
				conversion	selectivity				
neuron number	frequency	flow rate	power	CH_4	H_2	C_2H_2/C_2H_4	C_2H_6	C_3H_8	C_4H_{10}
1	0.073	0.213	−0.410	−0.275	−1.897	2.050	2.990	−2.208	−1.112
2	−0.797	−1.596	−3.649	−0.048	2.810	1.150	0.5907	2.0913	0.716
3	0.108	−3.207	−1.372	−0.471	−0.359	−0.202	−0.483	−0.826	−0.463
4	0.106	−2.407	1.428	0.730	−1.208	0.015	−0.348	2.163	−1.145
5	−0.116	0.871	0.472	0.370	−0.664	0.040	3.328	−3.070	−0.614
6	−0.247	−0.587	1.102	−0.714	0.048	0.421	−1.767	−0.802	−1.465
7	0.156	−0.586	1.102	−1.544	−0.383	0.133	−1.956	−1.866	−1.625
8	1.396	−2.397	0.666	−0.164	−0.166	−0.942	0.916	−2.778	1.062

dx.doi.org/10.1021/jp502557s | J. Phys. Chem. C 2014, 118, 10686−10693

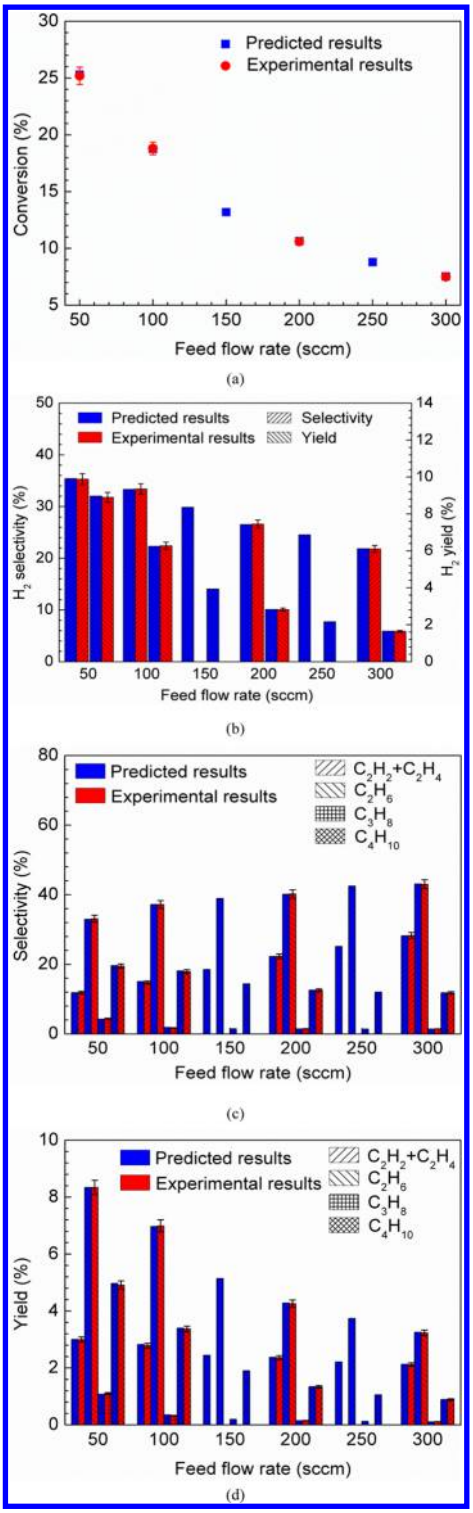

Figure 4. Effect of gas flow rate on (a) CH_4 conversion, (b) selectivity and yield of H_2, (c) selectivity of C_2−C_4 hydrocarbons, and (d) yield of C_2−C_4 hydrocarbons (frequency, 20 kHz; power, 45 W).

particularly for the conversion of CH_4. The conversion of CH_4 significantly decreases by a factor of 3 when the feed gas flow increases from 50 mL min^{-1} to 300 mL min^{-1}, which can be attributed to a decrease of the residence time of the feed gas in the discharge volume, resulting in a reduced chance for CH_4 to collide with energetic electrons and reactive species. Similar profiles for methane conversion have been reported in previous studies.[10,23] In addition, the yield of H_2 follows a tendency that is the same as that of CH_4 conversion and decreases from 8.9% to 1.6% with the increase of the feed flow rate to 300 mL min^{-1}. In contrast, the selectivity to C_2 hydrocarbons significantly increases with the gas flow rate, whereas the selectivity of C_3 and C_4 decreases by a factor of 3 with the rising in the gas flow. The optimized and well-trained ANN model enables us to predict the reaction performance of the plasma process at other flow rates (e.g., 150 mL min^{-1}), as plotted in Figure 4. The results suggest that a low feed flow rate is beneficial to improving the conversion of CH_4 and yield of gas products.

3.2.2. Effect of Discharge Power. A perfect match between the experimental and simulated data at different discharge powers (15−55 W) has been achieved, as shown in Figure 5. The discharge power is found to be the most influential parameter for the plasma processing of methane in terms of the conversion of CH_4 and selectivity of C_2−C_4 gas products. The conversion of CH_4 almost linearly increases with the increase of the plasma power, reaching a maximum value of 36% at a discharge power of 75 W, as predicted by the ANN model. In addition, the selectivity of H_2 increases by a factor of 2 to 44.7% while the yield of H_2 is significantly enhanced by four times when increasing the discharge power from 15 to 75 W. Increasing the discharge power is found to decrease the selectivity of C_2H_2 and C_2H_4 hydrocarbons by 30% but enhance the selectivity of saturated hydrocarbons (C_2H_6, C_3H_8, and C_4H_{10}) simultaneously. In this study, the maximum C_2 and C_4 selectivity of 53.3% and 25.6% can be obtained at a discharge power of 75 W, as predicted by the ANN model. Co-generation of hydrogen, C_2H_6, and C_4H_{10} can be achieved in the nonoxidative coupling of methane in a DBD reactor. These findings also suggest that increasing the plasma power inhibits the generation of light hydrocarbons and converts them to saturated hydrocarbons and hydrogen.

3.2.3. Effect of Frequency. The effect of the excitation frequency on the plasma nonoxidative conversion of methane has been evaluated, as shown in Figure 6. There is a good agreement between the experimental results and simulated results. In this study, the excitation frequency of the discharge is found to be the least important parameter affecting the plasma methane reaction. Changing the frequency from 20 to 50 kHz only slightly decreases the conversion of CH_4 by 10%. The simulation results show that the CH_4 conversion decreases to 16% when the excitation frequency is further increased to 70 kHz. The yield and selectivity of hydrogen follows a tendency similar to the conversion of CH_4 with the increase in frequency. In addition, the selectivity and yield of hydrocarbons (C_2−C_4) are found to be almost independent of the excitation frequency.

3.2.4. Energy Efficiency of the Plasma Process. The effect of discharge power, gas flow rate, and excitation frequency on the energy efficiency of the plasma nonoxidative conversion of CH_4 has been examined from both experimental and simulation approaches, as shown in Figure 7. There is a good agreement between the experimental results and simulated ones obtained from the well-trained ANN model. In this study, the discharge power is found to be the most important parameter affecting the energy efficiency of the CH_4 reaction. The energy efficiency for the conversion of CH_4 reaches a maximum value of 0.43 mmol/kJ and significantly decreases with increasing plasma power. The effect of the excitation frequency on the CH_4 conversion efficiency is very weak, which can be reflected by the sensitivity analysis of the processing parameters showing that the excitation frequency is the least important parameter for the

dx.doi.org/10.1021/jp502557s | J. Phys. Chem. C 2014, 118, 10686−10693

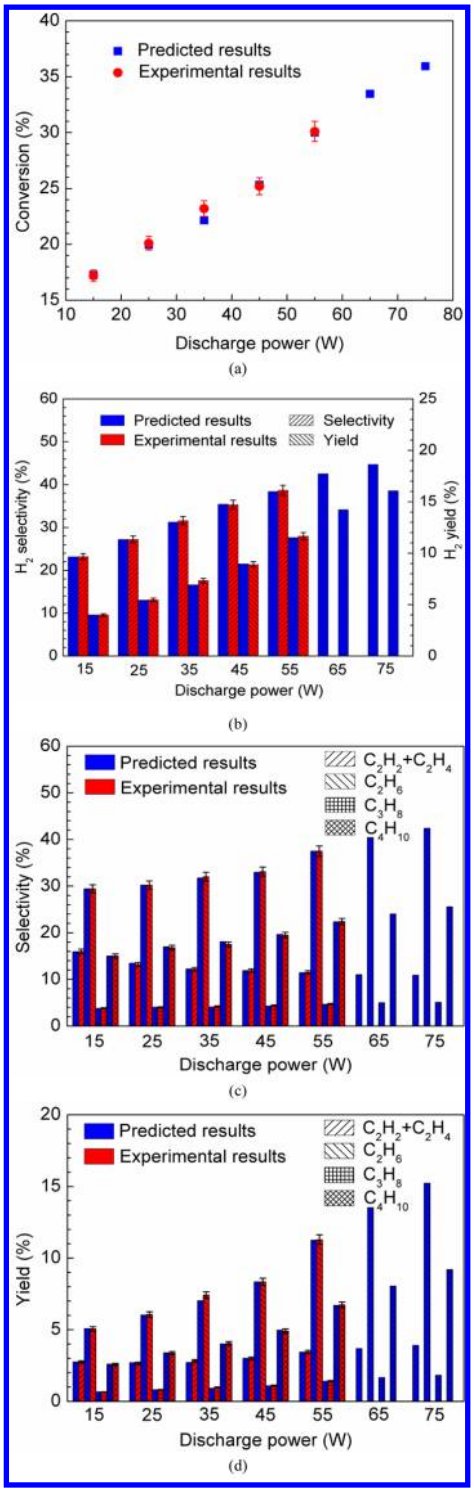

Figure 5. Effect of discharge power on (a) CH_4 conversion, (b) selectivity and yield of H_2, (c) selectivity of C_2−C_4 hydrocarbons, and (d) yield of C_2−C_4 hydrocarbons (frequency, 20 kHz; gas flow rate, 50 mL min^{-1}).

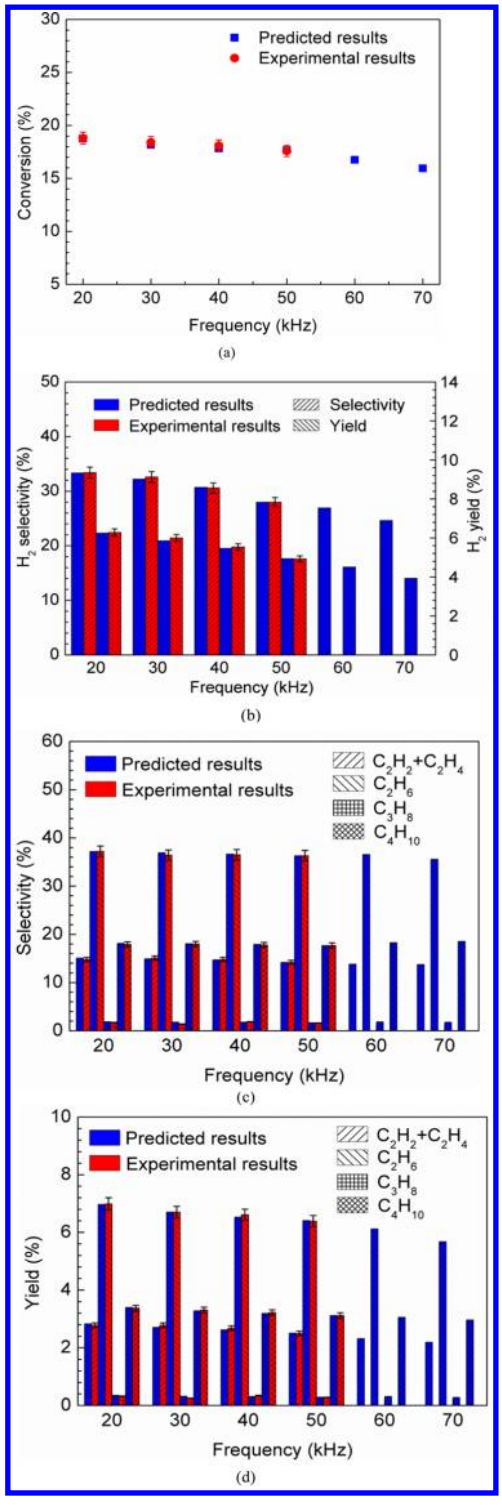

Figure 6. Effect of excitation frequency on (a) CH_4 conversion, (b) selectivity and yield of H_2, (c) selectivity of C_2−C_4 hydrocarbons, and (d) yield of C_2−C_4 hydrocarbons (discharge power, 45 W; gas flow rate, 100 mL min^{-1}).

plasma conversion of CH_4. The energy efficiency of the conversion is almost doubled when the gas flow rate increases from 50 mL min^{-1} to 300 mL min^{-1}, suggesting that the gas flow rate also plays an important role comparable to that of the discharge power in the plasma processing of methane.

3.2.5. Reaction Mechanisms. The nonoxidative conversion of methane without dilution by nonthermal plasmas is initiated by electron impact dissociation of CH_4 to generate CH_3, CH_2, and CH radicals (eqs 10−12), which induces subsequent recombination to form higher hydrocarbons or further decomposition through electron impact dissociation

$$CH_4(g) + e \rightarrow CH_3 + H + e \quad (10)$$

dx.doi.org/10.1021/jp502557s | J. Phys. Chem. C 2014, 118, 10686−10693

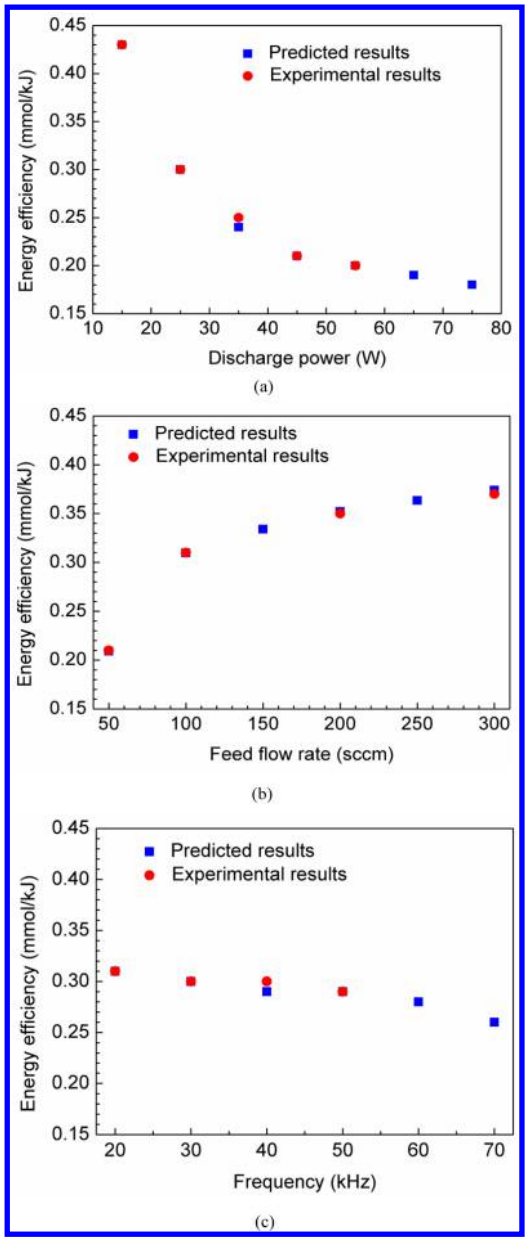

Figure 7. Effect of different processing parameters on the energy efficiency of the plasma methane conversion: (a) discharge power, (b) gas flow rate, and (c) excitation frequency.

$$CH_4(g) + e \rightarrow CH_2 + H_2(g) + e \quad (11)$$

$$CH_4(g) + e \rightarrow CH + H + H_2(g) + e \quad (12)$$

In the presence of higher energetic electrons (>14 eV), direct CH_4 decomposition occurs to produce H_2 and solid carbon:

$$CH_4(g) + e \rightarrow C(s) + 2H_2(g) + e \quad (13)$$

The above four reactions (eqs 10−13) are the major routes for CH_4 consumption and hydrogen production. This can be confirmed by a linear relationship between H_2 yield and CH_4 conversion. The distribution of the gas products in the plasma processing of CH_4 is related to the relative importance of different electron impact dissociations (eqs 10−12) and the yields of CH_x (x = 1−3) radicals, which are strongly dependent on the energy input and plasma reactor configuration. Yao et al. investigated the conversion of methane into acetylene and hydrogen by a high-frequency pulsed point-to-point plasma discharge with a high reaction temperature. They found that the major radicals from electron impact dissociation of CH_4 are CH and CH_2 based on the generation of gas products in their experiments.[26] Zhao et al. proposed that the dominant radicals formed in the conversion of methane by a pulsed corona discharge are CH radicals with a small number of CH_3 and CH_2 radicals because the measured concentration of C_2H_2 is much higher than that of C_2H_6 and C_2H_4 at an energy input of 384 mJ/pulse.[28] Yang suggested that there is a transition in which C_2H_2 will be the main product if the specific energy input increases to 100 eV/molecule.[23] Rueangjitt et al. reported that C_2H_2 is the main gas-phase hydrocarbon with a high selectivity of 70−90% in the methane-reforming reaction by a microscale AC gliding arc discharge, which suggests that CH from electron collision with CH_4 could be the dominant radical forming C_2H_2 because of a significantly higher energy density in the gliding arc.[12] In this work, we find that C_2H_6 is the main hydrocarbon instead of C_2H_2 and C_2H_4 at the energy inputs of 4.2−21 eV/molecule, which is consistent with previous experimental and modeling studies that C_2H_6 is the major hydrocarbon in either nonoxidative conversion of CH_4 or dry reforming of CH_4 using dielectric barrier discharges. Yang developed a plasma chemical kinetic model and demonstrated that a low-energy input (70 eV/molecule) leads to the formation of ethane as the main gas product.[23] The most important reaction path for C_2H_6 formation is from the methyl radical through the following neutral−neutral recombination

$$CH_3 + CH_3 \rightarrow C_2H_6 \quad (14)$$

Another important reaction route for the formation of C_2H_6 is CH_4 recombination with CH_2[23]

$$CH_4 + CH_2 \rightarrow C_2H_6 \quad (15)$$

De Bie et al. developed a 1D fluid model to simulate plasma conversion of CH_4 in a similar coaxial dielectric barrier discharge reactor at atmospheric pressure. The result has shown that the reaction (eq 10) is responsible for 79% of the total electron impact dissociation of CH_4, while the reactions shown in eqs 11 and 12 are responsible for only 15 and 5%, respectively.[36] This indicates that CH_3 is the major radical from the electron collision of methane in the dielectric barrier discharge, which reasonably explains why C_2H_6 is the main gas-phase hydrocarbon in the nonoxidative conversion of methane. Even at a low-energy input, there are enough CH_x (x = 1, 2, 3) radicals to form C_2H_6. C_2H_4 is formed either by electron impact dissociation of C_2H_6 or by recombination of CH_2 with itself, while C_2H_2 is formed mainly by electron impact dissociation of C_2H_4 or by recombination of CH.

Electron impact dissociation of C_2H_6 is believed to be the most important reaction pathway for the consumption of C_2H_6, leading to the formation of C_2H_4 and C_2H_5.

$$C_2H_6 + e \rightarrow C_2H_5 + H + 2e \quad (16)$$

$$C_2H_6 + e \rightarrow C_2H_4 + H_2 + 2e \quad (17)$$

C_2H_5 is an important radical to form C_3H_8 or C_4H_{10} through neutral−neutral recombination

$$C_2H_5 + CH_3 \rightarrow C_3H_8 \quad (18)$$

$$C_2H_5 + C_2H_5 \rightarrow C_4H_{10} \quad (19)$$

dx.doi.org/10.1021/jp502557s | J. Phys. Chem. C 2014, 118, 10686−10693

In this study, the yield of C_4H_{10} is found to be significantly higher than that of C_3H_8, suggesting that a large fraction of the C_2H_5 radical reacts with itself rather than with CH_3.

4. CONCLUSIONS

Co-generation of hydrogen and higher hydrocarbons from the nonoxidative coupling of methane has been achieved in a coaxial DBD reactor at atmospheric pressure and low temperatures (<80 °C). A three-layer BP neural network has been developed to simulate and predict the complex plasma methane reaction. The LM training algorithm combined with a tangent sigmoid transfer function (TANSIG) at the hidden layer with 8 neurons and a linear transfer function (PURELIN) at the output layer offers the optimal solution for the training of the BP neural network. There is a fairly good agreement between the experimental results and simulated data for the plasma processing of methane. The maximum CH_4 conversion of 36% with a high selectivity of C_2H_6 (42.4%) is obtained at a discharge power of 75 W, as predicted by the ANN model, while the energy efficiency for the plasma process reaches the highest level of 0.43 mmol/kJ at a discharge power of 15 W. The sensitivity analysis of three processing parameters shows that the discharge power plays the most important role with a relative weight of 45−52% in the plasma methane conversion process, while the excitation frequency of the plasma system is found to be the least important parameter and has a very weak effect on the reaction performance of the plasma methane process particularly on the selectivity of C_2−C_4 hydrocarbons. Our results have demonstrated that the optimized and well-trained ANN model offers a new and alternative route for effectively simulating and predicting the complex and nonlinear plasma methane process and for gaining a better understanding of the relative importance of the processing parameters in the plasma chemical reaction.

AUTHOR INFORMATION

Corresponding Author

*Tel.: +44-1517944513. Fax: +44-1517944540. E-mail: xin.tu@liv.ac.uk.

Notes

The authors declare no competing financial interest.

ACKNOWLEDGMENTS

Support of this work by the UK EPSRC and RAENG is gratefully acknowledged.

REFERENCES

(1) Gallon, H. J. Ph.D. Dissertation, The University of Manchester, Manchester, U.K., 2010.
(2) Intergovernmental Panel on Climate Change. http://www.ipcc.ch.
(3) Abbas, H. F.; Wan Daud, W. M. A. *Int. J. Hydrogen Energy* **2010**, *35*, 1160−1190.
(4) Hu, Y. H.; Ruckenstein, E. *Adv. Catal.* **2004**, *48*, 297−345.
(5) Yuliati, L.; Yoshida, H. *Chem. Soc. Rev.* **2008**, *37*, 1592−1602.
(6) Mizuno, A. *Catal. Today* **2013**, *211*, 2−8.
(7) Chen, H. L.; Lee, H. M.; Chen, S. H.; Chao, Y.; Chang, M. B. *Appl. Catal., B* **2008**, *85*, 1−9.
(8) Tao, X. M.; Bai, M. G.; Li, X.; Long, H. L.; Shang, S. Y.; Ying, Y. X.; Dai, X. Y. *Prog. Energy Combust. Sci.* **2011**, *37*, 113−124.
(9) Tu, X.; Gallon, H. J.; Twigg, M. V.; Gorry, P. A.; Whitehead, J. C. *J. Phys. D: Appl. Phys.* **2011**, *44*, 274007.
(10) Tu, X.; Whitehead, J. C. *Appl. Catal., B* **2012**, *125*, 439−448.
(11) Gallon, H. J.; Tu, X.; Whitehead, J. C. *Plasma Process Polym.* **2012**, *9*, 90−97.
(12) Rueangjitt, N.; Sreethawong, T.; Chavadej, S.; Sekiguchic, H. *Chem. Eng. J. (Amsterdam, Neth.)* **2009**, *155*, 874−880.
(13) Zou, J. J.; Zhang, Y. P.; Liu, C. J.; Li, Y.; Eliasson, B. *Plasma Chem. Plasma Process.* **2003**, *23*, 69−82.
(14) Li, X. S.; Lin, C. K.; Shi, C.; Xu, Y.; Wang, Y. N.; Zhu, A. M. *J. Phys. D: Appl. Phys.* **2008**, *41*, 175203.
(15) Gallon, H. J.; Tu, X.; Twigg, M. V.; Whitehead, J. C. *Appl. Catal., B* **2011**, *106*, 616−620.
(16) Chun, Y. N.; Yang, Y. C.; Yoshikawa, K. *Catal. Today* **2009**, *148*, 283−289.
(17) Tu, X.; Gallon, H. J.; Whitehead, J. C. *J. Phys. D: Appl. Phys.* **2011**, *44*, 482003.
(18) Tu, X.; Gallon, H. J.; Whitehead, J. C. *Catal. Today* **2013**, *211*, 120−125.
(19) Tu, X.; Verheyde, B.; Corthals, S.; Paulussen, S.; Sels, B. F. *Phys. Plasmas* **2011**, *18*, 080702.
(20) Paulussen, S.; Verheyde, B.; Tu, X.; De Bie, C.; Martens, T.; Petrovic, D.; Bogaerts, A.; Sels, B. F. *Plasma Sources Sci. Technol.* **2010**, *19*, 034015.
(21) Liu, C. J.; Mallinson, R.; Lobban, L. *J. Catal.* **1998**, *179*, 326−334.
(22) Liu, C. J.; Marafee, A.; Lobban, L. *Appl. Catal., A* **1999**, *178*, 17−27.
(23) Yang, Y. *Plasma Chem. Plasma Process.* **2003**, *23*, 327−346.
(24) Ghorbanzadeh, A. M.; Matin, N. S. *Plasma Chem. Plasma Process.* **2005**, *25*, 19−29.
(25) Matin, N. S.; Savadkoohi, H. A.; Feizabadi, S. Y. *Plasma Chem. Plasma Process.* **2008**, *28*, 189−202.
(26) Yao, S. L.; Suzuki, E.; Meng, N.; Nakayama, A. *Plasma Chem. Plasma Process.* **2002**, *22*, 225−237.
(27) Kado, S.; Urasaki, K.; Sekine, Y.; Fujimoto, K.; Nozaki, T.; Okazaki, K. *Fuel* **2003**, *82*, 2291−2297.
(28) Zhao, G. B.; John, S.; Zhang, J. J.; Wang, L. N.; Muknahallipatna, S.; Hamann, J. C.; Ackerman, J. F.; Argyle, M. D.; Plumb, O. A. *Chem. Eng. J. (Amsterdam, Neth.)* **2006**, *125*, 67−79.
(29) Indarto, A.; Choi, J. W.; Lee, H.; Song, H. K. *Energy* **2006**, *31*, 2986−2955.
(30) Xu, C.; Tu, X. *J. Energy Chem.* **2013**, *22*, 420−425.
(31) Jo, S. K.; Lee, D. H.; Kang, W. S.; Song, Y. H. *Phys. Plasmas* **2013**, *20*, 123507.
(32) Jo, S. K.; Lee, D. H.; Kang, W. S.; Song, Y. H. *Phys. Plasmas* **2013**, *20*, 083509.
(33) Wang, B. W.; Yan, W. J.; Ge, W. J.; Duan, X. F. *Chem. Eng. J. (Amsterdam, Neth.)* **2013**, *234*, 354−360.
(34) Yao, S. L.; Nakayama, A.; Suzuki, E. *AIChE J.* **2001**, *47*, 419−426.
(35) Aerts, R.; Tu, X.; Van Gaens, W.; Whitehead, J. C.; Bogaerts, A. *Environ. Sci. Technol.* **2013**, *47*, 6478−6485.
(36) De Bie, C.; Verheyde, B.; Marten, T.; van Dijk, J.; Paulussen, S.; Bogaerts, A. *Plasma Processes Polym.* **2011**, *8*, 1033−1058.
(37) De Bie, C.; Marten, T.; van Dijk, J.; Paulussen, S.; Verheyde, B.; Corthals, S.; Bogaerts, A. *Plasma Source Sci. Technol.* **2011**, *20*, 024008.
(38) Snoecks, R.; Aerts, R.; Tu, X.; Bogaerts, A. *J. Phys. Chem. C* **2013**, *117*, 4957−4970.
(39) Tu, J. V. *J. Clin. Epidemiol.* **1996**, *49*, 1225−1231.
(40) Nelson, M. M.; Illingworth, W. T. *A Practical Guide to Neural Nets*; Addison-Wesely: Boston, MA, 1991.
(41) Shen L., MSc Thesis, University of Liverpool, Liverpool, U.K., 2013.
(42) Elmolla, E. S.; Chaughuri, M.; Meselhy Eltoukhy, M. *J. Hazard. Mater.* **2010**, *179*, 127−134.
(43) Aleboyeh, A.; Kasiri, M. B.; Olya, M. E.; Aleboyeh, H. *Dyes Pigm.* **2008**, *77*, 288−294.